The B1.351 and P.1 variants extend SARS-CoV-2 host range to mice

Authors:

Xavier Montagutelli[1]*, Matthieu Prot[2], Laurine Levillayer[3], Eduard Baquero Salazar[4], Grégory Jouvion[5-6], Laurine Conquet[1], Flora Donati[7,8], Mélanie Albert[7,8], Fabiana Gambaro[2,9], Sylvie Behillil[7,8], Vincent Enouf[7,8], Dominique Rousset[10], Jean Jaubert[1], Felix Rey[4], Sylvie van der Werf[7,8], Etienne Simon-Loriere[2]*

Affiliations:

[1] Mouse Genetics Laboratory, Institut Pasteur, Paris, France
[2] Evolutionary Genomics of RNA Viruses, Institut Pasteur, Paris, France
[3] Functional Genetics of Infectious Diseases, Institut Pasteur, Paris, France
[4] Structural Virology, Institut Pasteur, Paris, France
[5] Ecole Nationale Vétérinaire, Unité d'Histologie et d'Anatomie Pathologique, Maisons-Alfort, France
[6] Université Paris Est Créteil, ENVA, ANSES, Unité DYNAMIC, Créteil, France
[7] Molecular Genetics of RNA viruses, CNRS UMR 3569, Université de Paris, Institut Pasteur, Paris, France
[8] National Reference Center for Respiratory Viruses, Institut Pasteur, Paris, France
[9] Université de Paris, Paris, France
[10] Institut Pasteur de la Guyane, Laboratoire de Virologie, Cayenne, French Guiana, France.

*Corresponding authors: xavier.montagutelli@pasteur.fr and etienne.simon-loriere@pasteur.fr

Keywords: SARS-CoV-2, variants, host range, mice

Abstract:

Receptor recognition is a major determinant of viral host range, as well as infectivity and pathogenesis. Emergences have been associated with serendipitous events of adaptation upon encounters with a novel host, and the high mutation rate of RNA viruses has been proposed to explain their frequent host shifts [1]. SARS-CoV-2 extensive circulation in humans has been associated with the emergence of variants, including variants of concern (VOCs) with diverse mutations in the spike and increased transmissibility or immune escape [2]. Here we show that unlike the initial virus, VOCs are able to infect common laboratory mice, replicating to high titers in the lungs. This host range expansion is explained in part by the acquisition of changes at key positions of the receptor binding domain that enable binding to the mouse angiotensin-converting enzyme 2 (ACE2) cellular receptor, although differences between viral lineages suggest that other factors are involved in the capacity of SARS-CoV-2 VOCs to infect mice. This abrogation of the species barrier raises the possibility of wild rodent secondary reservoirs and provides new experimental models to study disease pathophysiology and countermeasures.

Main Text:

Host range expansion or switch to other species has been prevalent in the course of coronaviruses evolutionary history [3]. Understanding the host range and how it is modified as the pathogen evolves is critical to estimate the emergence risk and determine the reservoirs to monitor. In the case of the severe acute respiratory syndrome coronavirus 2 (SARS-CoV-2), responsible for the ongoing coronavirus disease 2019 (COVID-19) pandemic, animals such as non-human primates, hamsters, ferrets, minks and cats were shown to be permissive [4]. By contrast, the zoonotic virus was shown to not replicate in mice and rats due to poor binding of the virus spike on the rodent cellular receptor angiotensin-converting enzyme 2 (ACE2).

At the end of 2020, the emergence of variants of concern (VOC) was noted in different parts of the world. The lineage B.1.1.7 (Pango designation [5], also named 20I/501Y.V1 or VOC202012/01) was noted for its rapid spread in the UK [6], while lineage B.1.351 (20H/501Y.V2) expanded in multiple regions of South Africa [7] and the P.1 (20J/501Y.V3) lineage emerged in Manaus, Brazil [8]. The global circulation and spread of these variants have led to concerns about increased transmission and their potential to evade immunity elicited by vaccination or naturally acquired. All three variants harbor the N501Y change in the spike glycoprotein which belongs to a set of 6 key amino acid residues critical for the tight interaction of the RBD with hACE2 [9]. Strikingly, this mutation was also noted, among others, in independently generated mouse-adapted SARS-CoV-2 strains [10,11]. Here, we assessed the replication potential in cells and in mice of low-passage clinical SARS-CoV-2 isolates of the main lineages.

The B.1.351 and P.1 variants efficiently replicate in mice airways

We first measured the capacity of a panel of low-passage clinical isolates belonging to the main lineage and to each of the VOCs lineages (Fig. S1) to infect mouse cells expressing the murine ACE2 receptor (DBT-mACE2), by comparison with VeroE6 cells. Contrary to the wild type viruses (B and B.1 lineages) which did not replicate in these cells, all VOCs viruses replicated to high titers at 48h post infection (Fig. S2).

We next inoculated 8-week-old BALB/c and C57BL/6 mice intranasally (i.n.) with a representative virus of either the most prevalent SARS-CoV-2 lineage (basal to B.1, carrying the D614G substitution) or the B.1.1.7, B.1.351 or P.1 lineages and we measured the viral load and titer in the lungs on day 3 post infection (dpi3). Consistently with what was reported for the ancestral virus [12], only low amounts of viral RNA and no live B.1 virus was detected (Fig. 1A-B). In contrast, inoculation with the B.1.351 or the P.1 viruses yielded high titer virus replication in lung tissues in both mouse strains. The viral load was significantly lower for the B.1.1.7 virus, with no infectious virus detected in the BALB/c lungs. To capture the time course of the productive infection with the B.1.351 and P.1 viruses, we also sampled infected mice at day 2 and 4, revealing an early peak of infection (Fig. S3). None of the mice infected with either viruses developed symptoms nor lost weight.

Three days after B.1.351 or B.1.1.7 virus inoculation, histological evaluation of the lung ranged from normal morphology to moderate lesions with multifocal interstitial infiltrates of lymphocytes, plasma cells, macrophages and rarer neutrophils, and degenerating epithelial cells in the bronchial and bronchiolar spaces. Anti-N immunohistochemistry revealed the presence of infected cells in bronchiolar epithelium, bronchiolar and alveolar spaces and alveolar walls (Figure 1C).

The ability of viruses of the B.1.351 and P.1 lineages to replicate in common laboratory mice extends the host range of SARS-CoV-2 at least to this species. It has been proposed that persistence

can select for host range expansion of animal viruses, by selecting for virus variants that recognize phylogenetic homologues of the receptor [13,14]. Interestingly, there is still speculation on the mechanism of emergence of the VOCs, which are all characterized by an unusually large number of mutations compared to their last common ancestor, including a number of changes (substitution and deletions) in the spike protein. While the genomic surveillance could have not captured all the evolutionary intermediates leading to these lineages, similar patterns of accumulated changes were noted in some longitudinal studies of immunocompromised individuals infected by SARS-CoV-2 for extended periods of time [15,16], leading to the hypothesis of a role of such long-term infections in their emergence. As mutations in the positions of interest in the spike RBD (417, 484 and 501), alone or in combination, have been noted in other lineages during the extensive circulation of SARS-CoV-2 in human populations [17], and associated in vitro with modification of the affinity for human ACE2, the observed host range expansion nevertheless likely represents only a serendipitous by-product of selection for increased transmissibility in its current host.

Mechanistically, while all VOCs appeared to be able to replicate in a mouse cell line expressing mACE2, we noted differences *in vivo*, with the B.1.1.7 virus inoculation yielding significantly lower viral load in the lungs than the B.1.351 and P.1 viruses. Homology modeling of the spike in contact with mACE2 reveals that the murine version of the receptor presents a strongly negatively charged central patch composed of residues E35, D37, D38 and Q42. These residues are also present in hACE2 but associated with several positively charged residues, which are replaced by more neutral amino acids in mACE2 (Figure 2B). This feature indicates that efficient binding to mACE2 would require complementary positive charges in the RBD. As expected, the mutation N501Y makes its local environment in the RBD more neutral and hides negative charges exposed in the B.1 RBD. The E484K mutation found in the RBD of variants B.1.351 and P.1 is also located in the ACE2 binding interface, resulting in a more positively charged RBD surface, in turn contributing to better binding to the negatively charged patch in mACE2, and might explain the differences observed *in vivo*. This interpretation is consistent with recent results obtained with pseudotyped viruses showing that the N501Y, E484K and their combination increase entry in mACE2 expressing cells [18]. However, other changes among the constellations defining the VOC lineages might also play a role in the resulting *in vivo* phenotype. Indeed, the mouse-adapted variants reported by Gu et al [10] and later Sun et al [19] induced pathological and inflammation features that were not observed here, and were also associated with genetic changes outside of the spike. Further studies are needed to dissect the combinatory role of the mutations defining the SARS-CoV-2 VOCs.

The ability of viruses of the B.1.351 or P.1 lineages to replicate in common laboratory mice will facilitate *in vivo* studies in this species, to evaluate countermeasures (vaccines or therapeutic interventions), to assess antibody cross-reactivity and vaccine cross-protection, and for functional studies using genetically altered mouse strains. Further in-depth studies will be needed to characterize the pathological consequences of infection with these variants. Notably, unlike what was described for a mouse adapted strain carrying the N501Y substitution [10], young adult mice infected with our variants showed no signs of disease nor body weight loss. Whether a more severe condition could be observed in older mice, in other mouse strains or with other isolates of the same lineages remains to be determined. In addition, the difference of responses noted between the BALB/c and C57BL/6 mice for the B.1.1.7 virus suggests a potential role of host factors as the amino acid sequence of their ACE2 is identical.

Finally, although the infectious dose and the transmissibility between mice remain to be established for these new variants, as well as the permissiveness of related animal species, these results raise major questions on the risk of mice or other rodents living in proximity to humans of becoming secondary reservoirs for SARS-CoV-2 in regions where the B.1.351, P.1 or other specific variants circulate, from where they could evolve separately and potentially spillback to humans. Indeed, rodents have been hypothesized as the ancestral host of some betacoronaviruses (lineage A, which includes the seasonal human coronaviruses OC43 and HKU1 [20,21]). While rodent densities are highly variable and more difficult to control, similar and actionable concerns were raised upon the detection of SARS-CoV-2 in Mink farms in The Netherlands [22] and in Denmark [23] due to the density of animals housed, and the detection of changes in the virus genome. We posit that host range should be closely monitored along the continued evolution of SARS-CoV-2.

References

1 Woolhouse, M. E., Haydon, D. T. & Antia, R. Emerging pathogens: the epidemiology and evolution of species jumps. *Trends Ecol Evol* **20**, 238-244, doi:10.1016/j.tree.2005.02.009 (2005).

2 WHO. Weekly epidemiological update - 25 February 2021. (WHO, WHO, 2021).

3 Cui, J., Li, F. & Shi, Z. L. Origin and evolution of pathogenic coronaviruses. *Nat Rev Microbiol* **17**, 181-192, doi:10.1038/s41579-018-0118-9 (2019).

4 Johansen, M. D. *et al.* Animal and translational models of SARS-CoV-2 infection and COVID-19. *Mucosal Immunol* **13**, 877-891, doi:10.1038/s41385-020-00340-z (2020).

5 Rambaut, A. *et al.* A dynamic nomenclature proposal for SARS-CoV-2 lineages to assist genomic epidemiology. *Nat Microbiol* **5**, 1403-1407, doi:10.1038/s41564-020-0770-5 (2020).

6 Rambaut, A. *et al.* Preliminary genomic characterisation of an emergent SARS-CoV-2 lineage in the UK defined by a novel set of spike mutations. (2020).

7 Houriiyah Tegally, E. W., Marta Giovanetti, Arash Iranzadeh, Vagner Fonseca, Jennifer Giandhari, Deelan Doolabh, Sureshnee Pillay, Emmanuel James San, Nokukhanya Msomi, Koleka Mlisana, Anne von Gottberg, Sibongile Walaza, Mushal Allam, Arshad Ismail, Thabo Mohale, Allison J Glass, Susan Engelbrecht, Gert Van Zyl, Wolfgang Preiser, Francesco Petruccione, Alex Sigal, Diana Hardie, Gert Marais, Marvin Hsiao, Stephen Korsman, Mary-Ann Davies, Lynn Tyers, Innocent Mudau, Denis York, Caroline Maslo, Dominique Goedhals, Shareef Abrahams, Oluwakemi Laguda-Akingba, Arghavan Alisoltani-Dehkordi, Adam Godzik, Constantinos Kurt Wibmer, Bryan Trevor Sewell, José Lourenço, Luiz Carlos Junior Alcantara, Sergei L Kosakovsky Pond, Steven Weaver, Darren Martin, Richard J Lessells, Jinal N Bhiman, Carolyn Williamson, View ORCID ProfileTulio de Oliveira. Emergence and rapid spread of a new severe acute respiratory syndrome-related coronavirus 2 (SARS-CoV-2) lineage with multiple spike mutations in South Africa. (2020).

8 Nuno R Faria *et al.* Genomic characterisation of an emergent SARS-CoV-2 lineage in Manaus: preliminary findings. (2021).

9 Yi, C. *et al.* Key residues of the receptor binding motif in the spike protein of SARS-CoV-2 that interact with ACE2 and neutralizing antibodies. *Cell Mol Immunol* **17**, 621-630, doi:10.1038/s41423-020-0458-z (2020).

10 Gu, H. *et al.* Adaptation of SARS-CoV-2 in BALB/c mice for testing vaccine efficacy. *Science* **369**, 1603-1607, doi:10.1126/science.abc4730 (2020).

11 Rathnasinghe, R. *et al.* The N501Y mutation in SARS-CoV-2 spike leads to morbidity in obese and aged mice and is neutralized by convalescent and post-vaccination human sera. *medRxiv*, 2021.2001.2019.21249592, doi:10.1101/2021.01.19.21249592 (2021).

12 Dinnon, K. H., 3rd *et al.* A mouse-adapted model of SARS-CoV-2 to test COVID-19 countermeasures. *Nature* **586**, 560-566, doi:10.1038/s41586-020-2708-8 (2020).

13 Baric, R. S., Sullivan, E., Hensley, L., Yount, B. & Chen, W. Persistent infection promotes cross-species transmissibility of mouse hepatitis virus. *J Virol* **73**, 638-649, doi:10.1128/JVI.73.1.638-649.1999 (1999).

14 Schickli, J. H., Zelus, B. D., Wentworth, D. E., Sawicki, S. G. & Holmes, K. V. The murine coronavirus mouse hepatitis virus strain A59 from persistently infected murine cells exhibits an extended host range. *J Virol* **71**, 9499-9507, doi:10.1128/JVI.71.12.9499-9507.1997 (1997).

15 Kemp, S. A. *et al.* SARS-CoV-2 evolution during treatment of chronic infection. *Nature*, doi:10.1038/s41586-021-03291-y (2021).

16 Choi, B. *et al.* Persistence and Evolution of SARS-CoV-2 in an Immunocompromised Host. *N Engl J Med* **383**, 2291-2293, doi:10.1056/NEJMc2031364 (2020).

17 (2021).

18 Li, Q. *et al.* No higher infectivity but immune escape of SARS-CoV-2 501Y.V2 variants. *Cell*, doi:10.1016/j.cell.2021.02.042 (2021).

19 Sun, S. *et al.* Characterization and structural basis of a lethal mouse-adapted SARS-CoV-2. *bioRxiv*, 2020.2011.2010.377333, doi:10.1101/2020.11.10.377333 (2020).

20 Lau, S. K. *et al.* Discovery of a novel coronavirus, China Rattus coronavirus HKU24, from Norway rats supports the murine origin of Betacoronavirus 1 and has implications for the ancestor of Betacoronavirus lineage A. *J Virol* **89**, 3076-3092, doi:10.1128/JVI.02420-14 (2015).

21 Tsoleridis, T. *et al.* Shared Common Ancestry of Rodent Alphacoronaviruses Sampled Globally. *Viruses* **11**, doi:10.3390/v11020125 (2019).

22 Oreshkova, N. *et al.* SARS-CoV-2 infection in farmed minks, the Netherlands, April and May 2020. *Euro Surveill* **25**, doi:10.2807/1560-7917.ES.2020.25.23.2001005 (2020).

23 Lassaunière R *et al.* Working paper on SARS-CoV-2 spike mutations arising in Danish mink, their spread to humans and neutralization data [Pre-print]. (2020).

Acknowledgments:

We are grateful to Dr Luis Enjuanes (National Center for Biotechnology, Spain) for the generous gift of the DBT cells expressing mACE2. We thank Hélène Huet (Unité d'Histologie et d'Anatomie pathologique, Ecole Nationale Vétérinaire d'Alfort) for the histological and immunohistochemical techniques and Dr Agnès Durand for technical support. We also thank the team of the core facility P2M (Institut Pasteur) for genomic sequencing. We acknowledge the authors, originating and submitting laboratories of the sequences from GISAID (Suppl. Table 1). We avoided any direct analysis of genomic data not submitted as part of this paper and used this genomic data only as background. This work used the computational and storage services (Maestro cluster) provided by the IT department at Institut Pasteur, Paris. FG is part of the Pasteur-Paris University (PPU) International PhD programme, BioSPC doctoral school.

Funding:

This work was supported by the « URGENCE COVID-19 » fundraising campaign of Institut Pasteur), the French Government's Investissement d'Avenir program, Laboratoire d'Excellence Integrative Biology of Emerging Infectious Diseases (Grant No. ANR-10-LABX-62-IBEID), the Agence Nationale de la Recherche (Grant No. ANR-20-COVI-0028-01) and the RECOVER project funded by the European Union's Horizon 2020 research and innovation programme under grant agreement No. 101003589. ESL acknowledges funding from the INCEPTION programme (Investissements d'Avenir grant ANR-16-CONV-0005).

Author contributions: XM and ESL designed and coordinated the study. MP, LL and LC performed in vitro experiments and viral quantification. XM, LC and JJ performed in vivo experiments. GJ performed histopathological analysis. EBS and FAR performed the structural analysis. ESL and FG performed the phylogenetic analysis. FD and MA isolated and produced the viral isolates under the supervision of SB, VE and SvdW. XM and ESL wrote and revised the manuscript with input from all authors.

Competing interests: The authors declare no competing interests.

Data and materials availability: All data are available in the main text or the supplementary materials.

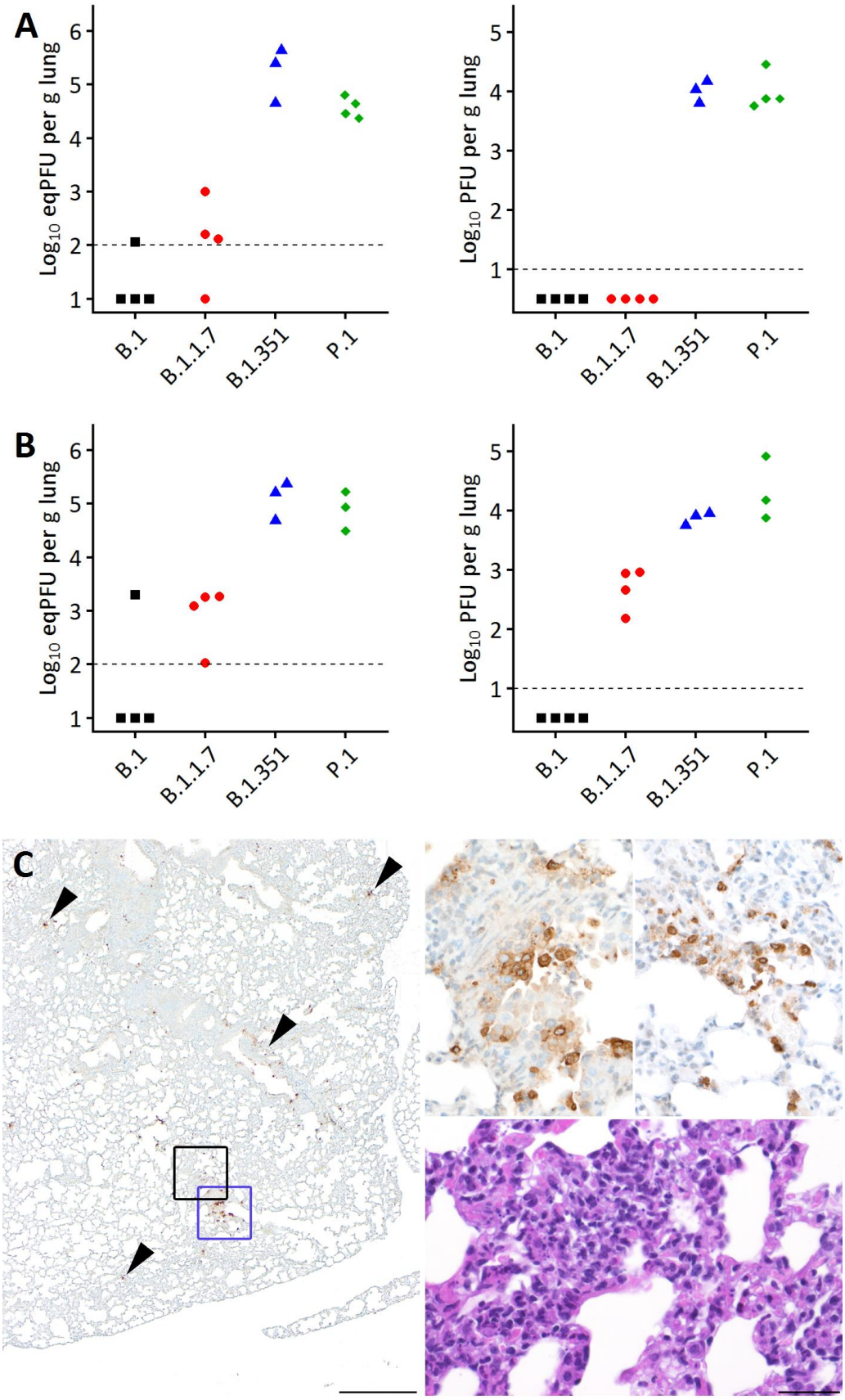
A
Log10 eqPFU per g lung
Log10 PFU per g lung
B.1
B.1.1.7
B.1.351
P.1
B
C

Fig. 1. SARS-CoV-2 B.1.351 and P.1 variants replicate to high titers in the lungs of young adult mice. Eight-week-old BALB/c (A) and C57BL/6 (B) mice were infected intranasally with $6x10^4$ PFU of SARS-CoV-2 isolates. Lungs were harvested at 3 dpi. Viral load was quantified by RT-qPCR. Viral titer was quantified on VeroE6 cells. The dotted line represents the limit of detection (LOD), and undetected samples are plotted at half the LOD. (C) Lung of a BALB/c mouse infected with B.1.351 SARS-CoV-2 variant. Detection of multifocal infected cells using anti N-immunohistochemistry, at a low magnification (left; black arrowheads; scale bar: 500 µm). High magnifications of bronchiolar wall (blue rectangle area; upper right) and alveoli (upper right). H&E staining (black rectangle area; bottom right; scale bar: 50 µm): interstitial infiltration of inflammatory cells (mononuclear cells and neutrophils).

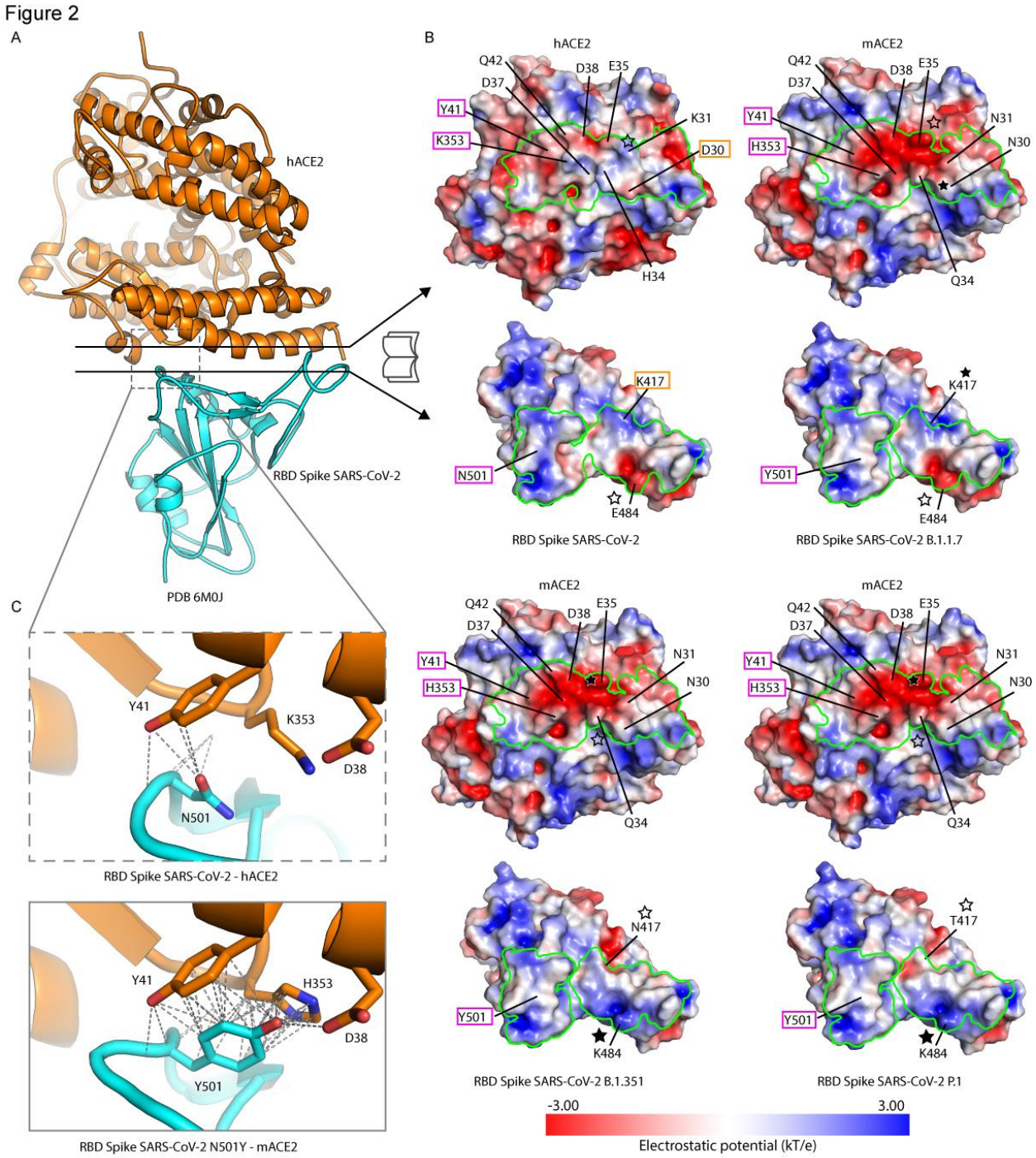

Fig. 2. Homology modeling of mouse ACE2 in complex with the RBD of SARS-CoV-2 variants.

A. Ribbon representation of the overall structure of the peptidase domain of hACE2 (orange) bound to SARS-CoV-2 spike RBD (cyan). **B.** Open book representations of the interacting surfaces between hACE2 and SARS-CoV-2 spike RBD (crystal structure 6M0J) and mACE2 with the RBDs of the B.1.1.7, B.1.351 and P.1 variants (homology models). The surfaces are coloured by electrostatic potential from red (negative charge, -3.00 kT/*e*) to blue (positive charge, 3.00 kT/*e*), as indicated by the coloured bar underneath. The green outline indicates the contact area between

the two molecules. The residues of the central negatively charged patch in ACE2 and the mutation sites in the RBDs are labelled. The residues in the RBD and in ACE2 that come into contact in the complex are labelled within boxes of the same colour. The stars indicate the RBD residues and their vicinity area in the interaction with ACE2. **C.** Detailed views of the interaction of the RBD residue N501 with hACE2 (PDB 6M0J, upper inset) and the mutant Y501 with mACE2 (homology model, lower inset). The dashed lines indicate possible electrostatic interactions between side and main chains. The model of the interaction of the N501Y RBD mutant with mACE2 indicates that the tyrosine side chain lies between the mACE2 residues Y41 and H353, making π-π interactions and a hydrogen bond with D38, suggesting a stronger interaction between mACE2 and RBDs carrying this mutation.

Supplementary Materials

Materials and Methods

Cells and viruses

VeroE6 cells (African green monkey kidney cells from ATCC (CCL-81)), A549-hACE2 cells (human adenocarcinoma alveolar epithelial cells expressing the human ACE2 receptor, a kind gift of Olivier Schwartz) and DBT-mACE2 cells (a kind gift of Dr Luis Enjuanes) were maintained in Dulbecco's Modified Eagle's Medium (DMEM) supplemented with 10% fetal bovine serum (FBS) and penicillin/streptomycin. A549-hACE2 cells were supplemented with 10 µg/ml of Blasticidin and DBT-mACE2 cells with 800 µg/ml of G418 to maintain the plasmid expressing ACE2.

B.1 strain: hCoV-19/France/GES-1973/2020, GISAID accession Id: EPI_ISL_414631; B.1.1.7 strain hcoV-19/France/IPP-00158i/2021, GISAID accession Id: EPI_ISL_1259025; B.1.351 strain hcoV-19/France/IDF-IPP00078/2021, GISAID accession Id: EPI_ISL_964916; and P.1 strain hCoV-19/FrenchGuiana/IPP03772/2021, GISAID accession Id: EPI_ISL_1096262. All SARS-CoV-2 isolates were supplied by the National Reference Centre for Respiratory Viruses hosted by Institut Pasteur (Paris, France) and headed by Pr. S. van der Werf. As previously described [1], the human sample from which strain hCoV-19/France/IDF-IPP158i/2020 was isolated has been provided by Dr. Karl Stefic et Pr Catherine Gaudy Graffin , CHRU de Tours, Tours, France and the human sample from which strain hcoV-19/France/IDF-IPP00078/2021 was isolated has been provided by Dr. Mounira Smati-Lafarge, CHI de Créteil, Créteil, France. The human sample from which strain hCoV-19/FrenchGuiana/IPP03772/2021 was isolated has been provided by Dr. Dominique Rousset, Institut Pasteur de la Guyane. This P.1 lineage virus was isolated by inoculation of VeroE6 cells, followed by two passages. Viruses were amplified and titrated by standard plaque forming assay on VeroE6 cells. The sequence of the stocks was verified by RNAseq on the mutualized platform for microbiology (P2M). All work with infectious virus was performed in biosafety level 3 containment laboratories at Institut Pasteur.

Phylogenetic analysis

We used the Nextstrain [2] pipeline (https://github.com/nextstrain/ncov) to reconstruct a global, representatively subsampled phylogeny highlighting the position of the isolates used in the experimental work. A maximum likelihood phylogenetic tree was built based on the GTR model, after masking 130 and 50 nucleotides from the 5' and 3' ends of the alignment, respectively, as well as single nucleotides at positions 18529, 29849, 29851, 29853. We checked for temporal signal using Tempest v1.5.3 [3]. The temporal phylogenetic analyses were performed with augur and TreeTime [4], assuming a clock rate of 830.0008±0.0004 (SD) substitutions/site/year [5], coalescent skyline population growth model and the root set on the branch leading to the Wuhan/Hu-1/2020 sequence. The time and divergence trees were visualized with FigTree v1.4.4 86 (http://tree.bio.ed.ac.uk/software/figtree/).

In vivo studies

Eight-week-old female BALB/cJRj (BALB/c) and C57BL/6JRj (C57BL/6) mice were purchased from Janvier Labs (Le Genest St Isle, France). Infection studies were performed in animal biosafety level 3 (BSL-3) facilities at the Institut Pasteur, in Paris. All animal work was approved

by the Institut Pasteur Ethics Committee (project dap 200008) and authorized by the French Ministry of Research under project 24613 in compliance with the European and French regulations.

Anesthetized (ketamine/xylazine) mice were infected intranasally with 6 x10^4 PFU of SARS-CoV-2 variants. Clinical signs of disease and weight loss were monitored daily. Mice were euthanized by ketamine/xylazine overdose at indicated time points (2, 3 or 4 days post infection - dpi) when samples for titer (right lung lobe) and histopathological analyses (left lung lobe) were collected. The left lung lobe was fixed by submersion in 10% phosphate buffered formalin for 7 days prior to removal from the BSL3 for processing. The right lung lobe was placed on a 70µ cell strainer (Falcon), minced with fine scissors and ground with a syringe plunger using 400 µl of PBS. Lung homogenates were used for viral quantification.

Histopathological analysis

Histological analysis was performed on paraffin-embedded 4µm-thick sections used for hematoxylin-eosin (H&E) staining and for the immunohistochemical detection of the virus, using a rabbit polyclonal primary antibody directed against SARS-CoV nucleocapsid (N) protein (Novus Biologicals, cat #NB100-56576; dilution: 1:200). The IHC were carried out based on the recommendations on the manufacturer's website (https://www.novusbio.com/products/sars-nucleocapsid-protein-antibody_nb100-56576).

Virus quantification.

Tissue homogenates were aliquoted for RNA quantification and titration. Viral RNA was extracted using the QIAamp viral RNA mini kit (Qiagen). Viral RNA quantification was performed by quantitative reverse transcription PCR (RT-qPCR) using the IP4 set of primers and probe as described on the WHO website (https://www.who.int/docs/default-34source/coronaviruse/real-time-rt-pcr-assays-for-the-detection-of-sars-cov-2-institut-35pasteur-paris.pdf?sfvrsn=3662fcb6_2) and the Luna Universal Probe One-Step RT-qPCR Kit (NEB).

For plaque assay, 10-fold serial dilutions of samples in DMEM were added onto VeroE6 monolayers in 24 well plates. After one-hour incubation at 37°C, the inoculum was replaced with 2% FBS DMEM and 1% Carboxymethylcellulose. Three days later, cells were fixed with 4% formaldehyde, followed by staining with 1% crystal violet to visualize the plaques.

Structural analysis

In order to study the effect on mACE2 binding of mutations in the RBD of the spike protein of the new SARS-CoV-2 variants, we generated a homology model for mACE2/RBD complex based on the available X-ray structure of the hACE2/RBD complex and analysed their electrostatic surface potential at neutral pH. We used this model to analyse the predicted electrostatic potential at the ACE2/RBD interface. We generated homology models of mACE2/RBD complexes corresponding to the various SARS-CoV-2 variants using the MODELLER software [6] based on the crystal structure of hACE2 peptidase domain in complex with SARS-CoV-2 spike RBD (PBD 6M0J). The quality of the models was inspected using PROCHECK and MOLPROBITY servers [7,8]. The surface electrostatic potential of the various models was calculated using the APBS/PDB2PQR server at pH 7.0 using a PARSE forcefield. The cartoon diagrams and surface representations were generated using PyMOL (Schrödinger, LLC)

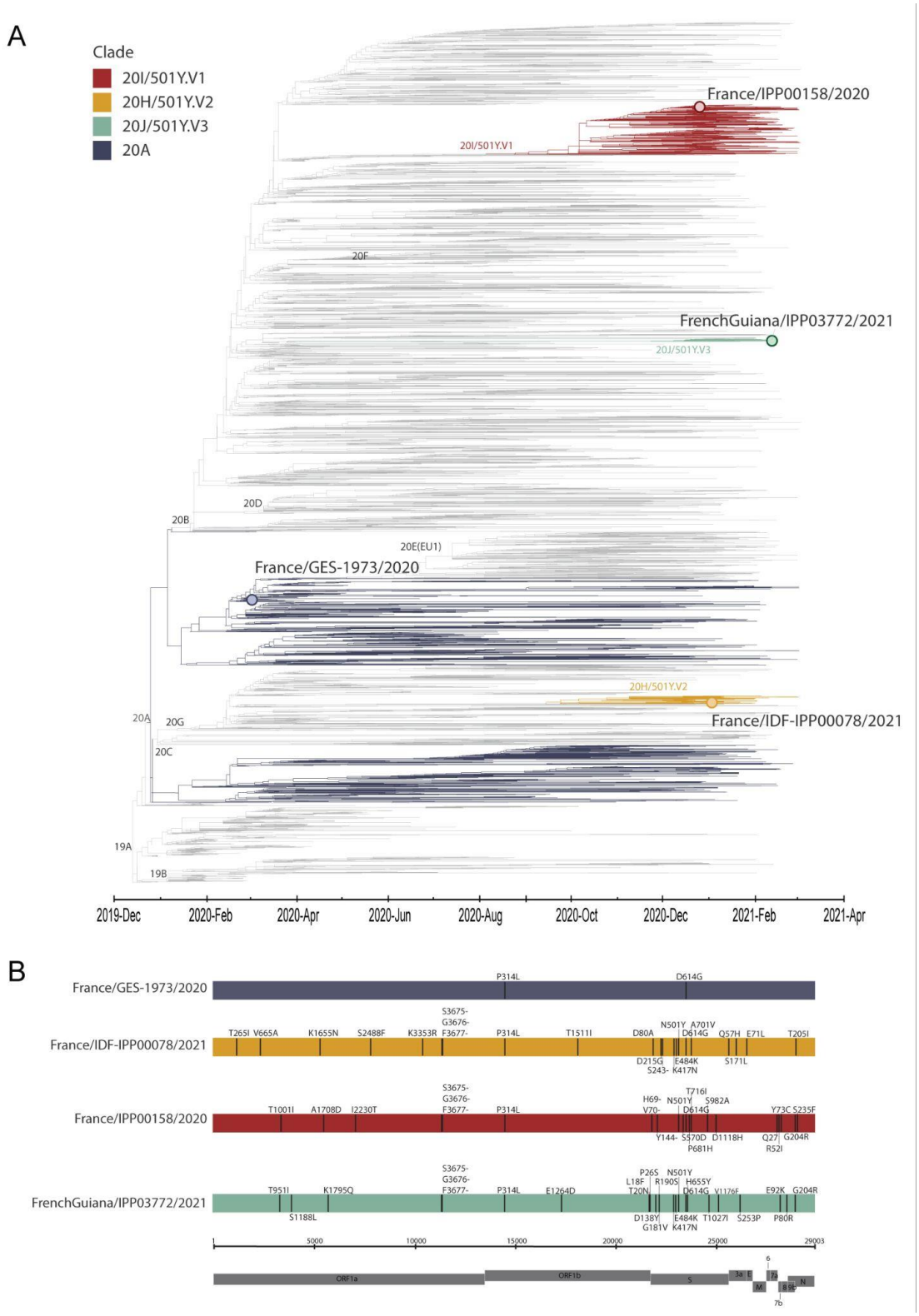

Fig. S1. SARS-CoV-2 isolates in a global context. Maximum likelihood phylogeny where the sequence corresponding to each variant is highlighted. Scheme of the variants in comparison to the ancestral sequence (NC_045512).

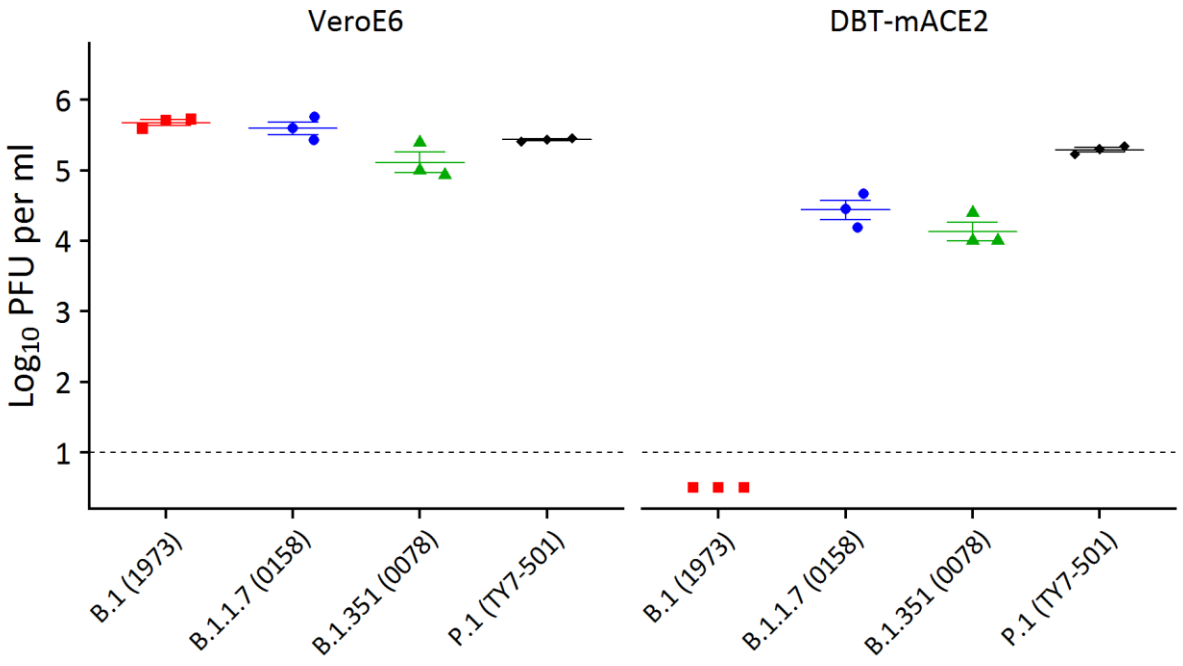

Fig. S2. SARS-CoV-2 variants show strong replication in VeroE6 cells and in a mouse cell line expressing mACE2. Viral titer in cell supernatant 48h after infection of A) Vero-E6 cell, B) DBT-mACE2 cell lines at a MOI = 0.1. Viruses were titrated on VeroE6 cells. The dotted line represents LOD, and undetected samples are plotted at half the LOD. While the B.1 virus did not replicate in DBT-mACE2 cells, all variants reached very high titers.

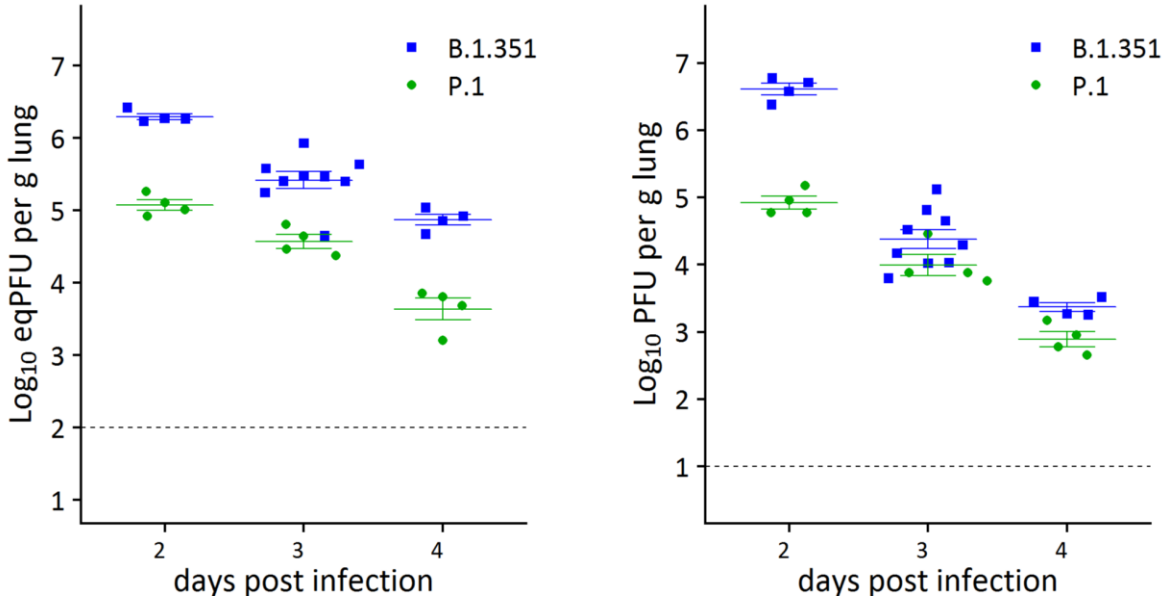

Fig. S3. Replication of SARS-CoV-2 B.1.351 and P.1 variants in lungs peaks at day 2 post infection in young adult BALB/c mice. Mice were infected intranasally with $6x10^4$ PFU of SARS-CoV-2 variants. Lungs were harvested at dpi 2, 3 and 4. Viral load was quantified by RT-qPCR (left). Viral titer was quantified on VeroE6 cells (right). The dotted line represents LOD.

Suppl Table 1. GISAID acknowledgements.

1 Planas, D. *et al.* Sensitivity of infectious SARS-CoV-2 B.1.1.7 and B.1.351 variants to neutralizing antibodies. *bioRxiv*, 2021.2002.2012.430472, doi:10.1101/2021.02.12.430472 (2021).

2 Hadfield, J. *et al.* Nextstrain: real-time tracking of pathogen evolution. *Bioinformatics* **34**, 4121-4123, doi:10.1093/bioinformatics/bty407 (2018).

3 Rambaut, A., Lam, T. T., Max Carvalho, L. & Pybus, O. G. Exploring the temporal structure of heterochronous sequences using TempEst (formerly Path-O-Gen). *Virus Evol* **2**, vew007, doi:10.1093/ve/vew007 (2016).

4 Sagulenko, P., Puller, V. & Neher, R. A. TreeTime: Maximum-likelihood phylodynamic analysis. *Virus evolution* **4**, vex042 (2018).

5 Rambaut, A. *Phylogenetic analysis of nCoV-2019 genomes*, <http://virological.org/t/phylodynamic-148analysis-176-genomes-6-mar-2020/3562020> (2020).

6 Webb, B. & Sali, A. Comparative Protein Structure Modeling Using MODELLER. *Curr Protoc Bioinformatics* **54**, 5 6 1-5 6 37, doi:10.1002/cpbi.3 (2016).

7 Laskowski, R. A., MacArthur, M. W. & Thornton, J. M. PROCHECK: validation of protein-structure coordinates. *International Tables for Crystallography*, 684-687, doi:https://doi.org/10.1107/97809553602060000882 (2012).

8 Williams, C. J. *et al.* MolProbity: More and better reference data for improved all-atom structure validation. *Protein Sci* **27**, 293-315, doi:10.1002/pro.3330 (2018).